STM JOURNALS

Journal of
Polymer & Composites

ISSN: 2321-2810 (Online)
ISSN: 2321-8525 (Print)
Volume 14, Special Issue 2, 2026
DOI (Journal): 10.37591/JoPC

https://journals.stmjournals.com/jopc

Research JoPC

Green Synthesis and Functional Evaluation of Ag–Polypyrrole/TeO_2 Nanocomposites for Advanced Electronic Applications

Kusuma D.[1], Revanasiddappa M.[2,*], Raghavendra N.[3], Y.T. Ravikiran Y.T.[4], Leela Kumar K.[5] and Swathi G.[6]

Abstract

Ag–PPy/TeO_2 nanocomposites with TeO_2 loadings ranging from 2% to 10% were synthesized using an in-situ chemical polymerization method. Green tea extract, rich in phytochemicals, acted as both a reducing and stabilizing agent to facilitate the formation of metal oxide nanoparticles. The structural and morphological characteristics of the nanocomposites were analyzed using FTIR, PXRD, and SEM techniques. FTIR confirmed the successful integration of Ag, TeO_2, and PPy functional groups. PXRD patterns indicated the crystalline nature of the composites, while SEM and EDX analyses verified uniform particle distribution and elemental composition. Electrical studies demonstrated significantly enhanced AC conductivity in all TeO_2-containing composites compared to pure Ag-decorated PPy. The improvement in charge transport with increasing TeO_2 content highlights the material's suitability for real-time sensing. Humidity-sensing evaluation revealed that the composite containing 6% TeO_2 exhibited superior response characteristics, making it the most promising candidate for practical sensor applications. Moreover, the excellent electrical behaviour of the developed composites suggests their potential for next-generation electronic and EMI-shielding devices.

***Author for Correspondence**
Revanasiddappa M.

[1]Research Scholar, Research Centre-Department of Chemistry, PES Institute of Technology Bangalore South Campus (PESIT–BSC), Bengaluru, Karnataka, India
[2]Professor, Department of Chemistry, PES University - Electronic City campus, Bengaluru, Karnataka, India
[3]Research Associate, Research Centre-Department of Chemistry, East West Institute of Technology, Bengaluru, Karnataka, India
[4]Professor, Department of Physics, Government First Grade College, Holalkere, Karnataka, India
[5]Associate Professor, Department of Mechanical Engineering, Vignan's Institute of Information Technology (A), Besides VSEZ, Vadlapudi Duvvada, Visakhapatnam, Andhra Pradesh, India
[6]Associate Professor, Department of Physics, Aditya Institute of Technology and Management (A), Tekkali, Srikakulam, Andhra Pradesh, India

Received Date: November 01, 2025
Accepted Date: December 11, 2025
Published Date: April 10, 2026

Citation: Kusuma D., Revanasiddappa M., Raghavendra N., Y.T. Ravikiran Y.T., Leela Kumar K. and Swathi G.. Green Synthesis and Functional Evaluation of Ag–Polypyrrole/TeO2 Nanocomposites for Advanced Electronic Applications. Journal of Polymer & Composites. 2026; 14(Special Issue 2): S64–S76p.

Keywords: TeO_2, green tea extract, AC conductivity, humidity sensing, EMI shielding

INTRODUCTION

Conducting polymers such as polyaniline (PANI), polypyrrole (PPy), polythiophene (PTP), and polyfuran (PFu) have attracted substantial interest due to their π-electron conjugated structure and versatile physicochemical properties. Among them, PPy stands out owing to its high electrical conductivity, environmental stability, low cost, and ease of synthesis [1–3]. Composites of PPy have been synthesized through chemical and electrochemical routes [4–6] with various organic and inorganic materials, including metal oxides, carbon nanotubes, and nanoparticles. These hybrid structures often demonstrate enhanced electrical behavior, charge retention, thermal stability, and mechanical robustness.

Despite these advantages, many PPy composites suffer from limited flexibility due to the rigid, fully conjugated backbone. However, extensive π-

electron delocalization across the pyrrole ring promotes high stability and enables strong interaction with dopants [7–9], leading to derivatives well suited for electronic and optoelectronic functions. For instance, poly(3-alkylthiophene) synthesized by direct oxidation of 3-alkylthiophene with $FeCl_3$ exhibits useful electrical and optical activity [10] and has been incorporated into various advanced composites [11, 12]. Thiophene-based hybrid materials have been reported at both micro- and nanoscales for applications such as sensors, energy devices, and flexible electronics [13–15]. Thus, PPy and related composites remain a promising class of materials for molecular electronics. Tellurium oxide (TeO_2) serves as an attractive filler due to its amphoteric nature and superior acousto-optic properties, mechanical durability, and chemical stability [16–18]. It is widely applied in deflectors, modulators, X-ray detectors, and gas-sensing components. TeO_2-based glasses and films are also of great interest for optical waveguides because of their high acousto-optic efficiency relative to other amphoteric oxides [19–21].

In light of this, the current research was carried out to investigate the synthesis and characterization of PPy composites containing tellurium oxide, as well as the behaviour of these composite materials in terms of their electrical conductivity. The newly synthesized material has been described using a variety of spectroscopic methods, and the conductivity of the material has been measured using four-probe conductivity meters. To synthesise a ternary composite, TeO_2 was added to the Ag-PPy binary composite. The electrical conductivity of ternary composites made of Ag-PPy/TeO_2 was optimized. Since mechanical mixing increases electrical conductivity and is cost-effective for mass manufacturing of nanocomposites, it was used to manufacture this ternary composite as a first attempt. FTIR, XRD, and FESEM were used to analyze the materials' structures and morphologies, respectively. In this study, we examined the AC electrical conductivity and EMI shielding effect of Ag-PPy/TeO_2 ternary composites with varying concentrations. First attempts at increasing AC conductivity and EMI shielding via the interfacial effects of the ternary composite (Ag-PPy/TeO_2) were made. The charge transport mechanism in Ag-PPy/TeO_2 composites was determined by comparing activation energies from AC conductivity tests.

EXPERIMENTAL

Materials

Pyrrole monomer (98%) was purchased from Sigma-Aldrich. TeO_2 and all analytical-grade reagents were procured from S.D. Fine Chemicals, Mumbai, India. Double-distilled water was used in all experiments.

PREPARATION OF GREEN TEA EXTRACT

A total of 4.2 g of chopped green tea leaves was mixed with 150 mL of distilled water in a 250 mL conical flask and heated at 80 °C for ~5 min. After brewing, the extract was filtered through Whatman No. 41 paper using a Buchner funnel. The filtrate contained phytochemicals such as polyphenols, terpenoids, reducing sugars, and amino acids, enabling its role as a green reducing/stabilizing agent [22].

SYNTHESIS OF PPY

Silver nitrate (5 g in 20 mL H_2O) acted as a precursor for in-situ oxidative polymerization. A total of 50 mL of green tea extract was added under constant stirring at room temperature. Pyrrole (1 mL) was added dropwise over 2–3 hours. The reaction mixture gradually transitioned to a dark green suspension, confirming polymerization. TeO_2 was then added in different proportions, and stirring continued for 24 h (Figure 1 and Table 1). The final product was filtered, washed repeatedly, and dried in a vacuum oven at 90 °C for 1 h. The resulting powder was used for further analyses.

MEASUREMENTS

XRD patterns were recorded using a PW 1719 diffractometer with Cu Kα radiation (λ = 1.5406 Å). Surface morphology was examined using a Hitachi SEM Model S-3600 N. FTIR spectra were recorded using a Perkin-Elmer RX-1 spectrometer with KBr pellets.

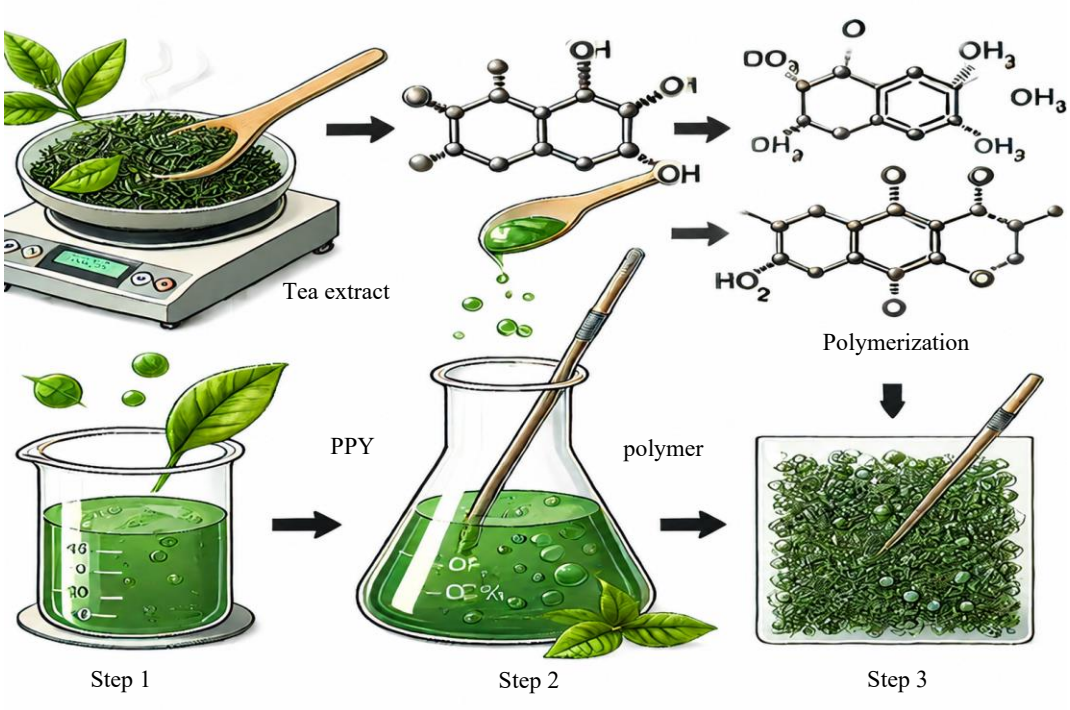

Figure 1. Schematic representation of the preparation of PPy.

Table 1. The volume of green tea extract was used in the synthesis of Ag-PPy/TeO_2 nanocomposites by varying the weight percentage of TeO_2.

Green tea extract (mL)	$AgNO^3$ Solution (Moles)	Volume of PPy (mL)	Weight of TeO_2 (mg)	Yield of Ag-PPy/TeO_2 (g)	Samples code
50 ml	1.53 M	1.0	5.00	1.32	Ag-PPy/2% TeO_2
50 ml	1.53 M	1.0	10.0	1.22	Ag-PPy/4% TeO_2
50 ml	1.53 M	1.0	15.0	1.32	Ag-PPy/6% TeO_2
50 ml	1.53 M	1.0	20.0	1.43	Ag-PPy/8% TeO_2
50 ml	1.53 M	1.0	25.0	1.56	Ag-PPy/10% TeO_2

TGA was conducted in an argon atmosphere from room temperature to 1000 °C at 10 °C/min using TA Instruments (V4.1). Pellets for electrical measurements were prepared via hydraulic pressing. A Keithley 2400 instrument was employed for conductivity studies at room temperature.

RESULTS AND DISCUSSIONS

XRD Studies

Figures 2(a)–(c) show the XRD patterns of TeO_2, Ag–PPy, and Ag–PPy/TeO_2 composites. Sharp and intense diffraction peaks confirmed the crystalline nature of TeO_2. The reflections at $2\theta \approx 27°$, 38°, 48°, 55°, and 68° were attributed to the tetragonal phase of TeO_2, which matched well with the standard JCPDS card (No. 42-1365) [23]. The Ag–PPy pattern exhibited characteristic peaks corresponding to Ag nanoparticles, along with a broad hump that indicated the amorphous structure of PPy. The peaks at $2\theta \approx 38°$, 44°, 64°, and 77° were indexed to the (111), (200), (220), and (311) planes of face-centered cubic Ag nanoparticles (JCPDS No. 04-0783).

The composite spectrum retained the characteristic peaks of both TeO_2 and Ag NPs, confirming the successful incorporation of these phases into the PPy matrix. In addition, the broad hump located between 15–30° persisted, demonstrating that the amorphous nature of PPy was preserved in the composite.

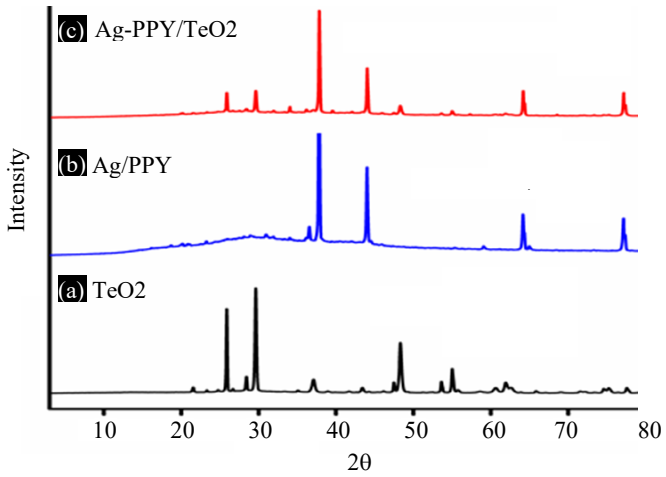

Figure 2. XRD patterns of a) TeO_2, b) Ag-PPy, and c) Ag-PPy/TeO_2 composites.

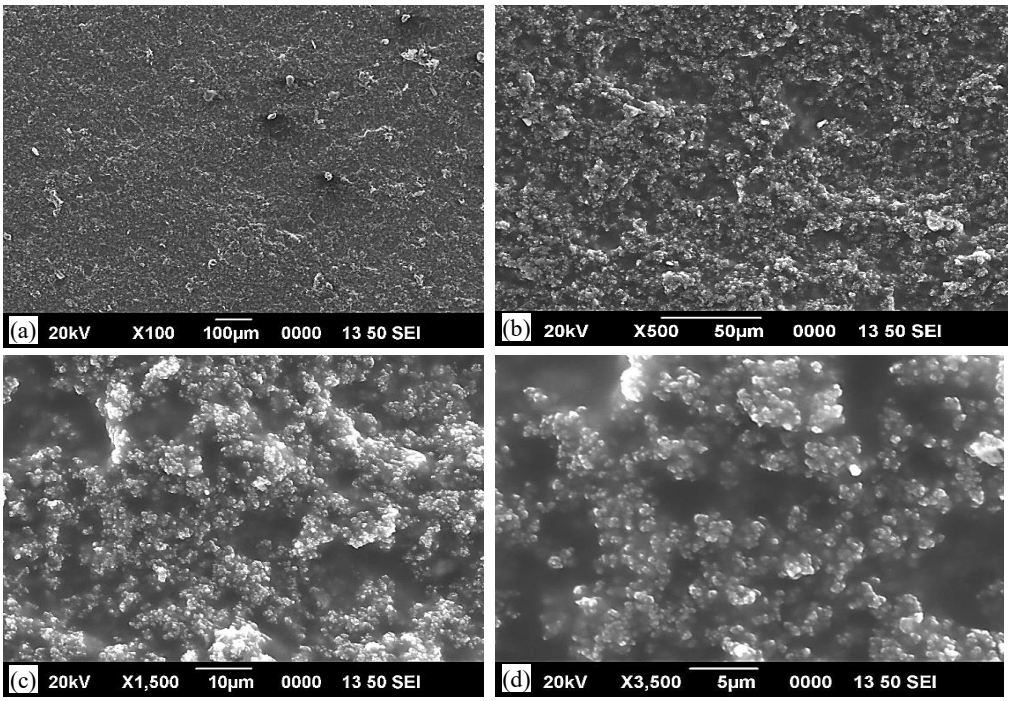

Figure 3. SEM micrographs of a) TeO_2, b) Ag-PPy, c) and d) Ag-PPy/TeO_2 composites.

SEM STUDIES

Figures 3(a–d) show the FESEM images of the Ag–PPy/TeO_2 composites. The Ag–PPy sample exhibited a small, compact granular morphology. Upon the introduction of TeO_2, the particles became more densely packed, and TeO_2 appeared to be uniformly distributed throughout the PPy matrix. These observations confirmed the successful incorporation of TeO_2 into the Ag–PPy structure. Furthermore, the doping led to a more compact morphology, indicating enhanced interfacial interaction within the composite.

FTIR STUDIES

Analysis of the FTIR spectra of Ag–PPy, TeO_2, and Ag–PPy/TeO_2 composites (Figure 4) showed that the incorporation of TeO_2 into the polymer matrix altered the characteristic absorption peaks of Ag–PPy. Ag–PPy exhibited typical vibrational bands between 1500 and 500 cm^{-1}, corresponding to C=C, C–N, and C–H bond vibrations in polypyrrole [24]. A broad peak near ~3400 cm^{-1} indicated N–H or O–H stretching vibrations commonly observed in doped polypyrrole.

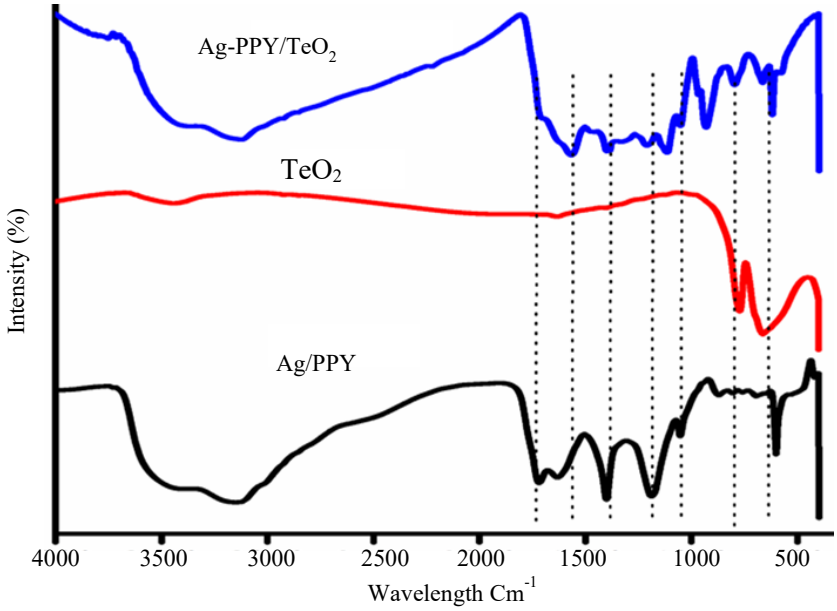

Figure 4. FTIR patterns of TeO_2, Ag-PPy, and Ag-PPy/TeO_2 composites.

For TeO_2, distinct absorption bands appeared in the 500–700 cm^{-1} region due to Te–O bond vibrations. These features were still visible in the composite spectrum, although with slightly reduced intensity compared to pure TeO_2. The characteristic Ppy peaks in the 1500–1000 cm^{-1} region remained prominent, confirming the retention of the polymer structure. Additionally, a broad absorption band between ~3500 and 3000 cm^{-1} suggested the presence of hydrogen bonding or residual O–H/N–H groups. Overall, the FTIR spectra verified the coexistence of Ag–PPy and TeO_2 within the composite. The preserved vibrational modes of both constituents indicated successful chemical integration, which may contribute to improved electrical conductivity and stability in the resulting nanocomposite.

THERMOGRAVIMETRIC ANALYSIS (TGA)

Figure 5 shows the thermogravimetric curves of TeO_2, Ag–PPy, and Ag–PPy/TeO_2 composites. In the thermogram of PPy, an initial weight loss of approximately 3% was observed near room temperature due to the evaporation of physically adsorbed water [25]. The mass remained nearly constant up to ~200 °C, after which a major thermal degradation occurred, leading to a weight loss of nearly 97% and indicating the complete decomposition of PPy by ~580°C, leaving no solid residue.

For the Ag–PPy/TeO_2 composite, a small initial mass loss of ~5.6% from room temperature to 100°C was attributed to moisture removal. The curve remained relatively stable until ~200 °C, followed by a second major degradation stage that resulted in a weight loss of ~63.8% between 200–450 °C due to the decomposition of PPy chains and the release of C, H, and N components. Beyond 450 °C, the mass showed only minimal change until ~760 °C, confirming the thermal stability of the inorganic TeO_2 component within the composite. A residual mass of ~21% was retained at 760 °C, whereas pure PPy left no residue, confirming the successful incorporation of thermally stable TeO_2 in the polymer matrix. These results demonstrated that the Ag–PPy/TeO_2 composite possessed enhanced thermal stability compared to pristine PPy.

AC CONDUCTIVITY STUDIES

Figures 6(a, b) show the variation of AC conductivity with frequency (log F) for Ag–PPy/TeO_2 composites containing 2–10 wt.% TeO_2. At low frequencies, the conductivity remained nearly constant due to high grain boundary resistance, which limited charge carrier movement. With increasing frequency, the AC conductivity increased for all composites, following the universal power law behavior typical of disordered conducting polymers [26].

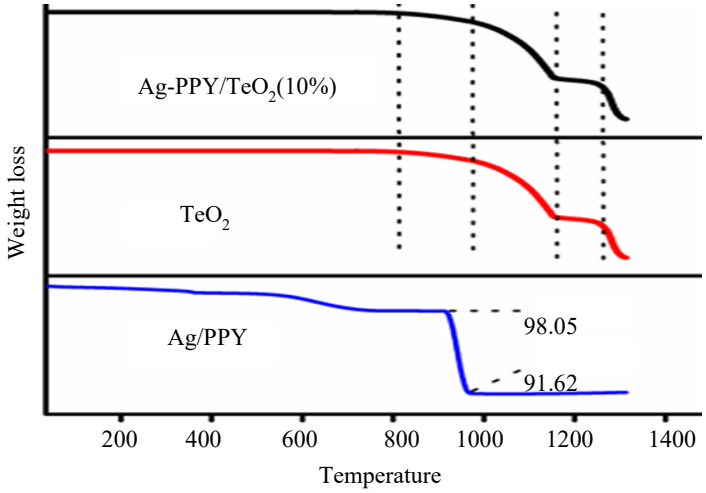

Figure 5. TGA patterns of TeO_2, AgPPy, and AgPPy/TeO_2 composites.

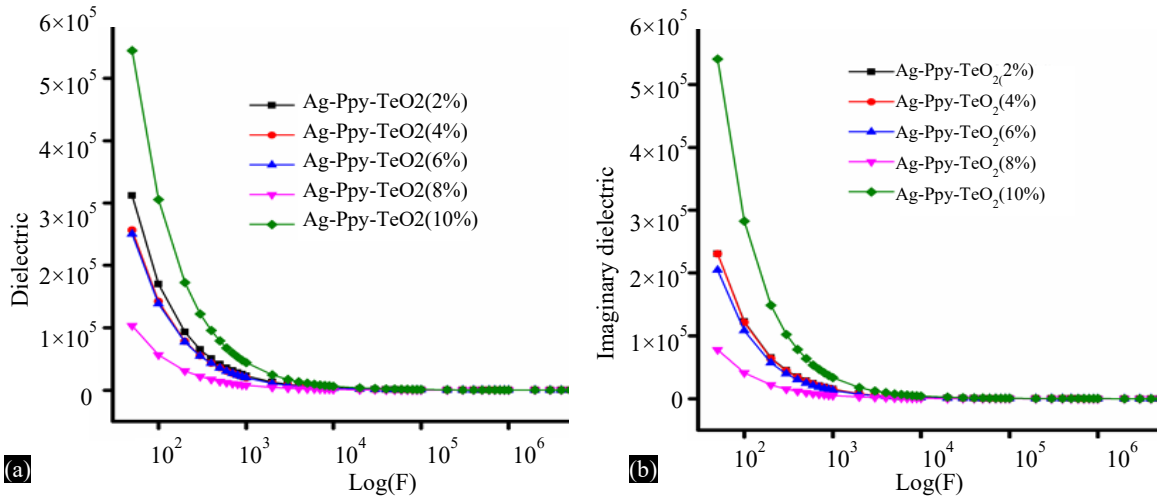

Figure 6. (a, b) Real and Imaginary AC conductivities of Ag-PPy/TeO_2 composites.

Four-probe measurements revealed that the conductivity of pristine PPy was 0.83×10^{-9} S cm^{-1}, while the incorporation of TeO_2 increased the conductivity to 1×10^{-5} S cm^{-1}. Among all samples, the 10 wt.% TeO_2 composite exhibited the highest conductivity, whereas the 2 wt.% composite showed the lowest. This enhancement was attributed to improved charge carrier pathways and increased interfacial polarization provided by TeO_2. At lower frequencies, polarization and space-charge accumulation restricted electron/ion mobility, resulting in lower conductivity [27]. At higher frequencies, the applied field enabled charge carriers to respond more effectively, thus enhancing conductivity. The observed frequency-dependent behavior suggested a hopping conduction mechanism, where charge carriers transitioned between localized states. The improved conductivity in higher TeO_2-loaded composites indicated their potential suitability for applications such as energy storage, humidity sensing, and gas-sensing devices Figure 6(b).

Figures 7(a, b) show the dielectric constant (real and imaginary components) as a function of frequency (log F). The 10 wt.% TeO_2 composite displayed the highest dielectric loss, while the 2 wt.% sample exhibited the lowest. Both dielectric components decreased sharply at low frequencies and tended to become constant at higher frequencies. Increasing TeO_2 content consistently enhanced polarization and charge storage capability. The rapid dielectric drops at low frequencies indicated a dielectric relaxation phenomenon associated with interfacial polarization. At higher frequencies, slower polarization mechanisms were unable to follow the alternating field, leading to stabilized dielectric behavior.

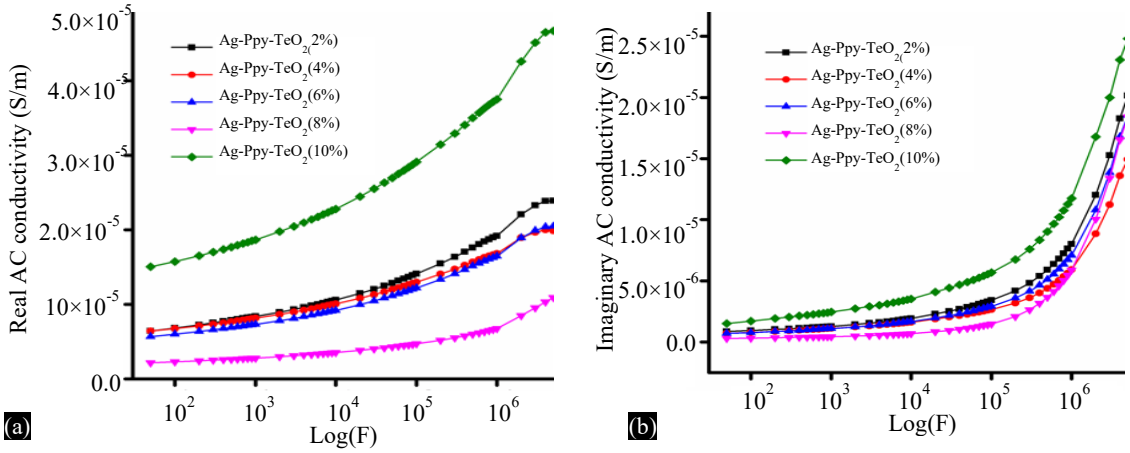

Figure 7. (a, b) Real and imaginary Dielectric constants of Ag-PPy/TeO_2 composites.

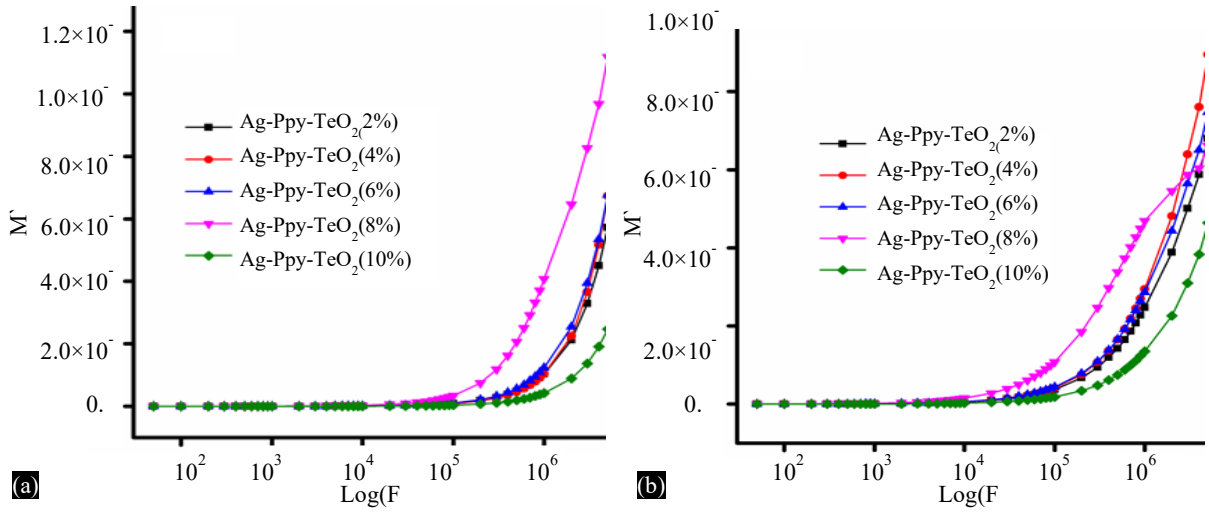

Figure 8. (a) Real and (b) Imaginary Electrical Modulus of Ag-PPy/TeO_2 composites.

Figure 8(a) shows the variation of the real and imaginary components of the electric modulus as a function of frequency (log F) for the Ag–PPy/TeO_2 composites. The real part of the electric modulus (M′) increased gradually with frequency for all samples. At low frequency regions, M′ remained almost constant and close to zero, indicating a negligible contribution to the overall dielectric response. At higher frequencies, the composite with 10 wt.% TeO_2 exhibited the lowest M′ values, while the 6 wt.% sample showed the highest. The imaginary component (M″) rose sharply with increasing frequency (Figure 8b). All composites displayed a relaxation peak in the high-frequency region, although with slight variations depending on TeO_2 loading. The relaxation phenomenon was most prominent for the 6 wt.% composite, whereas the 10 wt.% sample showed a comparatively weaker peak.

Figures 9(a, b) show the loss tangent (tan δ) for different TeO_2 contents. At low and intermediate frequencies, conduction, vibrational, and interfacial polarization losses contributed to the dielectric loss values. At higher frequencies, vibrational losses became the dominant factor [28]. The tan δ values decreased with frequency for all compositions (Figure 9(a)). Samples containing higher TeO_2 content (8 wt.% and 10 wt.%) demonstrated higher loss tangent values at low frequencies, indicating improved energy dissipation capability. At high frequencies, tan δ values converged, becoming nearly identical among all compositions.

As shown in Figure 9(b), AC conductivity increased with TeO_2 loading, reaching a maximum at 8 wt.% before slightly decreasing at 10 wt%. Conductivity remained significantly higher at 1 MHz and 10 MHz than at low frequencies, confirming enhanced charge transport at high frequency ranges.

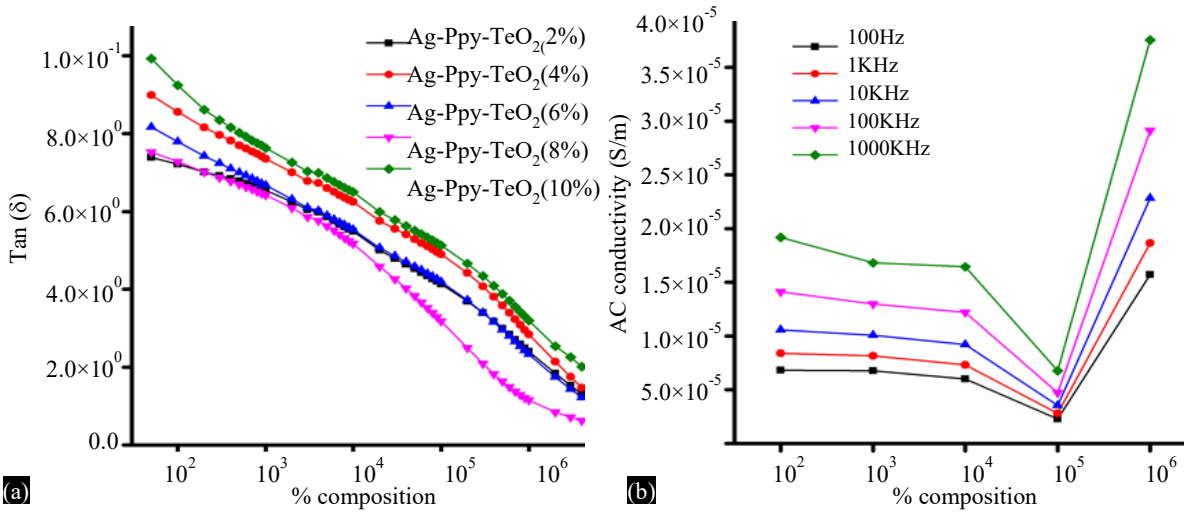

Figure 9. (a) and (b) tan (δ) and percentage composition of Ag-PPy/TeO_2.

These results indicated that both TeO_2 concentration and applied frequency significantly influenced the dielectric performance and AC conductivity of the composites, with the 8 wt.% TeO_2 material being the most promising for practical dielectric and sensing applications.

HUMIDITY SENSORS STUDIES

Figures 10(a–d) show the humidity response and hysteresis behavior of Ag–PPy/TeO_2 composites with varying TeO_2 contents (2–10 wt.%). As relative humidity (RH) increased, the resistance of all composites decreased, indicating a typical humidity-sensing response. Composites with higher TeO_2 content, particularly the 10 wt.% sample, exhibited a steeper decline in resistance, suggesting enhanced sensitivity to humidity variations [29–30]. In contrast, the 2 wt.% composite showed a smaller resistance change, indicating lower sensitivity. The dynamic humidity-response characteristics of the 6 wt.% TeO_2 composite are shown in Figure 10(b). When RH increased, resistance dropped sharply and returned close to its initial value once RH decreased, confirming reversible chemisorption behavior. The repeated cycling demonstrated stable and reproducible sensing performance with minimal hysteresis [31–32], highlighting the composite's reliability for real-time humidity monitoring.

Figure 10(c) presents the resistance variation of the 6 wt.% composite over the RH range of 11–97%. The resistance decreased almost linearly with increasing RH, confirming strong sensitivity and indicating a predictable humidity-dependent response suitable for practical sensor calibration. Figure 10(d) shows the logarithmic fit between resistance and RH for the same sample. The obtained slope value (3.067) indicated high sensitivity toward humidity changes. The strong correlation between RH and resistance validated the consistent behavior and measurement accuracy of the composite. Overall, the sensitivity of the Ag–PPy/TeO_2 composites increased with TeO_2 content. Among all compositions, the 6 wt.% sample demonstrated the most desirable combination of sensitivity, linearity, repeatability, and rapid recovery, confirming its potential as a high-performance humidity-sensing material.

STUDIES ON EMI SHIELDING EFFECTIVENESS

Electromagnetic interference shielding effectiveness (EMI SE) is an important parameter that represents a material's ability to block or attenuate electromagnetic radiation [33]. The three phenomena of reflection (SE_R), absorption (SE_A), and multiple reflection (S_M) are combined to form the electromagnetic interference shielding effectiveness (EMISE total), which is expressed as:

$$SE_T = SE_R + SE_A + SE_M \quad (1)$$

The Equation $SE_R = 10 \log_{10} (1\text{-}R)$ reflection (R) and transmission (T) are such that A+R+T = 1.

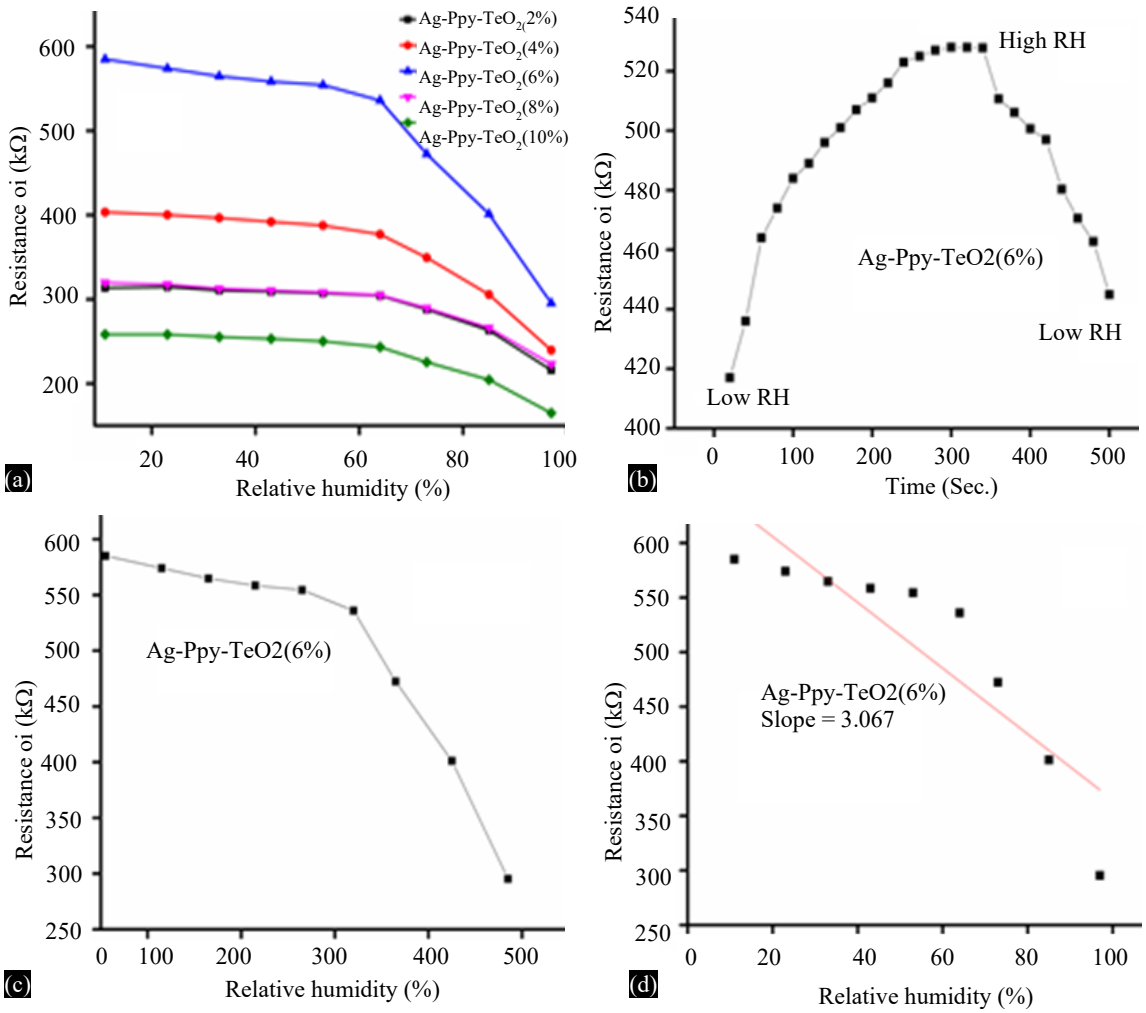

Figure 10. Humidity hysteresis and recovery response of a) Ag-PPy/TeO_2, b) Ag-PPy with 6% TeO_2, c) and d) Ag-PPy with 6% TeO_2 composite.

Total electromagnetic shielding effectiveness can be expressed as,

$$SE = -10 \log(P_T/P_I) = -20 \log (E_T/E_I) \quad (2)$$

Where P_I (E_I) and P_T (E_T) are the incident and transmitted powers of electromagnetic waves, respectively.

Figures 11(a, b) show the EMI SE of the Ag–PPy/TeO_2 (10 wt.%) composites with different thicknesses (3, 5, and 7 mm) in the frequency range of 2–3 GHz. All samples exhibited wave-like variations in SE with frequency. The EMI SE increased with TeO_2 incorporation, indicating that the addition of TeO_2 enhanced electrical conductivity and electromagnetic wave attenuation. Among the tested samples, the 3 mm thick composite demonstrated the highest EMI SE, as shown in Table 2, likely due to improved electrical conduction pathways and interfacial polarization. Reflection contributed more significantly to the total EMI SE compared with multiple reflections and absorption. To better interpret signal attenuation inside the waveguide, the free-space path loss formula was applied in the analysis. The EMI SE values of the Ag–PPy/TeO_2 composites varied notably within the tested GHz range, confirming that TeO_2 acted as an effective filler for improving the shielding performance of the polymer matrix. Overall, the Ag–PPy/TeO_2 composite showed promising potential for GHz-frequency EMI shielding applications due to its favourable electrical characteristics and structural design.

Table 2. EMI shielding effectiveness (dB) for different thicknesses of Ag-PPy/TeO_2 composites

Composites	Thickness of the film in mm	Frequency in G (Hz)	EMI shielding effectiveness SE total (dB)
Ag-PPy/TeO_2	3	2.8	-39
	5	2.8	-29
	7	2.8	-36

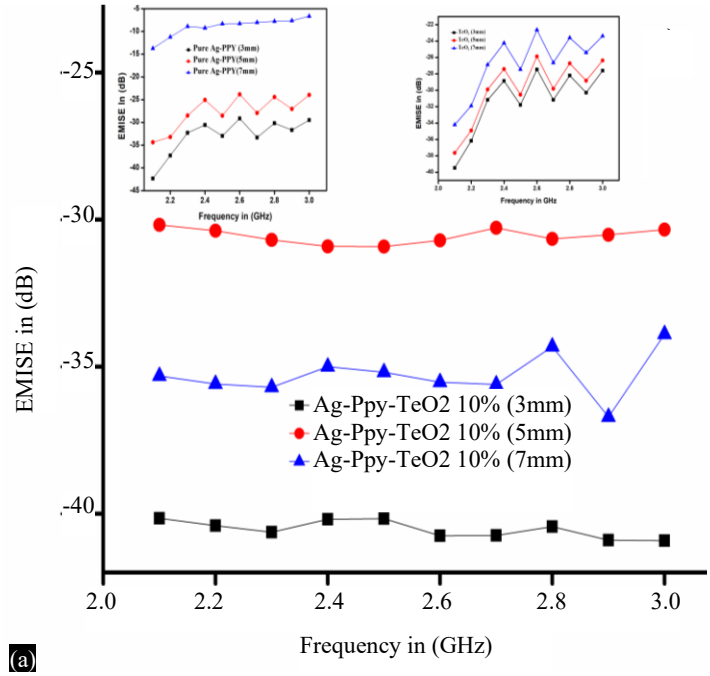

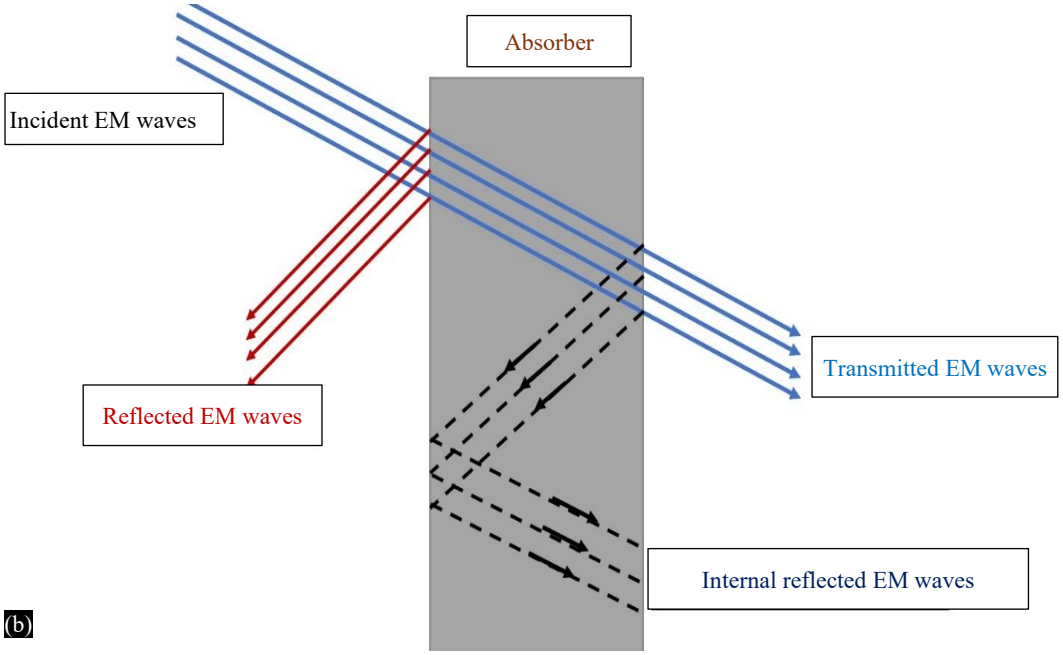

Figure 11. EMISE of (a) AgPPy with 10% wt.% TeO_2 composite and (b) EMI shielding.

CONCLUSION

This study systematically investigated the humidity-sensing properties of Ag–PPy/TeO_2 composites synthesized with different TeO_2 contents (2–10 wt.%). The electrical measurements revealed that the resistance of the composites decreased significantly with increasing relative humidity (RH), demonstrating strong humidity-sensing capability. Increasing TeO_2 content enhanced water adsorption

and charge carrier mobility due to the higher number of active sites, which led to improved conductivity. Among all compositions, the 6 wt.% TeO_2 composite exhibited the most favourable combination of sensitivity, linearity, and sensing range, confirming its promise for accurate humidity monitoring. The dynamic response studies showed rapid and reversible sensing behavior with good repeatability under cyclic RH variations. The logarithmic relationship between resistance and RH for the 6 wt.% composite provided a reliable basis for sensor calibration. Furthermore, AC conductivity and dielectric studies indicated improved charge-transport characteristics with increasing TeO_2 loading, supporting the composite's suitability for real-time monitoring applications.

Additionally, the 10 wt.% TeO_2 composite with a 3 mm thickness demonstrated significantly enhanced EMI shielding effectiveness in the 2–3 GHz frequency range, ascribed to improved electrical properties and interfacial interactions. In conclusion, the Ag–PPy/TeO_2 composites show excellent potential for multifunctional device applications, particularly in humidity sensing and EMI shielding systems. These findings pave the way for the development of advanced sensing materials for environmental monitoring, industrial control, and healthcare applications. Future work may focus on long-term stability, temperature effects, and scalable fabrication for commercial deployment.

Acknowledgement

The authors gratefully acknowledge PES University, Electronic City Campus, for providing financial support through the Internal Research Funding Program (PESUIRF/Chemistry-ECC/2020/14, dated 30-09-2020) to carry out this research. The authors also extend their gratitude to the Vision Group on Science and Technology, Bangalore, Karnataka (GRD-363).

REFERENCES

1. Joulazadeh M, Navarchian AH. Ammonia detection of one-dimensional nano-structured polypyrrole/metal oxide nanocomposite sensors. Synth Met. 2015; 210(B): 404–11. https://doi.org/10.1016/j.synthmet.2015.10.026
2. Dai T, Yang X, Lu Y. Conductive composites of polypyrrole and sulfonic-functionalized silica spheres. Mater Lett. 2007; 61(14–15): 3142–5. https://doi.org/10.1016/j.matlet.2006.11.012
3. Majid K, Awasthi S, Singla ML. Low temperature sensing capability of polyaniline and Mn_3O_4 composite as NTC material. Sens Actuators A Phys. 2007; 135(1): 113–8. https://doi.org/10.1016/j.sna.2006.06.055
4. Yuan L, Wang J, Chew SY, Chen J, Guo ZP, Zhao L, Konstantinov K, Liu HK. Synthesis and characterization of SnO_2–polypyrrole composite for lithium-ion battery. J Power Sources. 2007; 174(2): 1183–7. https://doi.org/10.1016/j.jpowsour.2007.06.179
5. Armelin E, Pla R, Liesa F, Ramis X, Iribarren JI, Alemán C. Corrosion protection with polyaniline and polypyrrole as anticorrosive additives for epoxy paint. Corros Sci. 2008; 50(3): 721–8. https://doi.org/10.1016/j.corsci.2007.10.006
6. Kim JY, Kim KH, Kim KB. Fabrication and electrochemical properties of carbon nanotube/polypyrrole composite film electrodes with controlled pore size. J Power Sources. 2008; 176(1): 396–402. https://doi.org/10.1016/j.jpowsour.2007.09.117
7. Chew SY, Guo ZP, Wang JZ, Chen J, Munroe P, Ng SH, Zhao L, Liu HK. Novel nano-silicon/polypyrrole composites for lithium storage. Electrochem Commun. 2007; 9(5): 941–6. https://doi.org/10.1016/j.elecom.2006.11.028
8. Wang J, Xu Y, Chen X, Sun X. Capacitance properties of single-wall carbon nanotube/polypyrrole composite films. Compos Sci Technol. 2007; 67(14): 2981–5. https://doi.org/10.1016/j.compscitech.2007.05.015
9. Majid K, Tabassum R, Shah AF, Ahmad S, Singla ML. Comparative study of synthesis, characterization and electrical properties of polypyrrole and polythiophene composites with tellurium oxide. J Mater Sci Mater Electron. 2008; 10: 958–66. https://doi.org/10.1007/s10854-008-9817-8

10. Niemi VM, Knuuttila P, Österholm J-E, Korvola J. Polymerization of 3-alkylthiophenes with $FeCl_3$. Polymer. 1992; 33(7): 1559–62. https://doi.org/10.1016/0032-3861(92)90138-M
11. Xie HQ, Liu CM, Guo JS. Preparation of conductive polypyrrole composites by in-situ polymerization. Polym. Int. 1999; 48(11): 1099–107. https://doi.org/10.1002/(SICI)1097-0126(199911)48:11<1099::AID-PI271>3.0.CO;2-P
12. Ballav N, Biswas M. Preparation and evaluation of a nanocomposite of polythiophene with Al_2O_3. Polym Int. 2003; 52(1): 179–84. https://doi.org/10.1002/pi.1001
13. Wang D, Wang Y, Li X, Luo Q, An J, Yue J. Sunlight photocatalytic activity of polypyrrole–TiO_2 nanocomposites prepared by 'in situ' method. Catal Commun. 2008; 9(6): 1162–6. https://doi.org/10.1016/j.catcom.2007.10.027
14. Vu QT, Pavlik M, Hebestreit N, Rammelt U, Plieth W, Pfleger J. Nanocomposites based on titanium dioxide and polythiophene: Structure and properties. React Funct Polym. 2005; 65(1–2): 69–77. https://doi.org/10.1016/j.reactfunctpolym.2004.11.011
15. Kong F, Wang Y, Zhang J, Xia H, Zhu B, Wang Y, Wang S, Wu S. Preparation and gas sensitivity study of polythiophene/SnO_2 composites. Mater Sci Eng B. 2008; 150(1): 6–11. https://doi.org/10.1016/j.mseb.2008.01.003
16. Kotov V, Shkerdin G, Shkerdin D, Kotov E. Multiphonon Bragg scattering of light in single-crystal paratellurite. J Opt Technol. 2005; 72: 511–4. https://doi.org/10.1364/JOT.72.000511
17. Arshak K, Korostynska O. Gamma radiation dosimetry using tellurium dioxide thin film structures. Sensors. 2002; 2: 347–55. https://doi.org/10.3390/s20800347
18. Dewan N, Sreenivas K, Gupta V. Properties of crystalline γ-TeO_2 thin film. J Cryst Growth. 2007; 305(1): 237–41. https://doi.org/10.1016/j.jcrysgro.2007.03.054
19. Yin HR, Jiang JS. Synthesis and characterization of γ-Fe_2O_3–polythiophene nanocomposites. J Mater Sci. 2005; 40: 3013–5. https://doi.org/10.1007/s10853-005-2380-2
20. Geetha S, Trivedi DC. A new route to synthesize high-degree polythiophene in a room-temperature melt medium. Synth Met. 2005; 155(1): 232–9. https://doi.org/10.1016/j.synthmet.2005.08.003
21. Wang TM, Liu WM, Tian J, Shao X, Sun DC. Electrical and thermal properties of carbon nanotube/epoxy composites. Polym Compos. 2004; 25: 111.
22. Kumar NN, Kumar PK, Revanasiddappa M. Study of mechanical and thermal properties of banana carbon composites of epoxy resin. AIP Conf Proc. 2020; 2274: 030029. https://doi.org/10.1063/5.0022486
23. Siciliano T, Tepore A, Micocci G, Genga A, Siciliano M, Filippo E. Transition from n- to p-type electrical conductivity induced by ethanol adsorption on α-tellurium dioxide nanowires. Sens. Actuators B Chem. 2009; 138(1): 207–13. https://doi.org/10.1016/j.snb.2009.02.007
24. Abdullah HS. Electrochemical polymerization and Raman study of polypyrrole and polyaniline thin films. Int. J. Phys. Sci. 2012; 7(38): 5468–76. https://doi.org/10.5897/IJPS12.529
25. Omastová M, Rychlý J, Trchová M, Kovářová J. Properties and thermal decomposition of polypyrrole prepared in the presence of sodium bis(2-ethylhexyl) sulfosuccinate. Des Monomers Polym. 2004; 7: 633–46. https://doi.org/10.1163/1568555042474220
26. Zeshan M, Ali M, Alanazi MM, Abdelmohsen SM, Khosa RY, Al-Sehemi AG, Ansari MZ, Tayeb RA, Tahir Farid HM, Rahman MM. Study of $SrEr_{0.04}Fe_{1.96}O_4$/PANI nanocomposites for high-frequency applications. Ceram Int. 2023; 49: 20536–43. https://doi.org/10.1016/j.ceramint.2023.03.183
27. Revanasiddappa M, Siddalinga Swamy D, Vinay K, Ravikiran YT, Raghavendra SC. Synthesis, characterization and DC conductivity studies of conducting polyaniline/PVA/fly ash polymer composites. AIP Conf Proc. 2018; 1953: 090070. https://doi.org/10.1063/1.5032917
28. Hameed AS, Bahiraei H, Reddy MV, Shoushtari MZ, Vittal JJ, Ong CK, Chowdari BV. Lithium storage properties of pristine and (Mg, Cu) co-doped $ZnFe_2O_4$ nanoparticles. ACS Appl Mater Interfaces. 2014; 6(13): 10744–53. https://doi.org/10.1021/am502605s
29. Madesh Kumar M, Patil PK, Lakshmi K, Reddy S, Manjunatha S, Ravikiran YT, Revanasiddappa M. Polythiophene/reduced graphene oxide nanocomposites for humidity sensing application. Mater Sci Forum. 2023; 1099: 45–50. https://doi.org/10.4028/p-KID2Pk

30. Patel B, Basavaraja M, Revanasiddappa M, Rangaswamy DR. Synthesis, transport, and electromagnetic shielding properties of Fe-PPy-SnO_2 nanocomposites. J Electron Mater. 2022; 51: 6937–50. https://doi.org/10.1007/s11664-022-09924-w
31. Naveen Kumar TG, Revanasiddappa M, Chethan B, Megha R, Chandrasekhar T, Prashantkumar M, Ravikiran YT, Devenrappa H. Humidity sensing performance of polypyrrole-based ternary composite. AIP Conf. Proc., 2020; 2244: 110015. https://doi.org/10.1063/5.0010282
32. Vinay K, Revanasiddappa M, Shivakumar K, Ravikiran YT, Manjunath S. Room temperature humidity sensing behaviour of silver-decorated polyaniline composite. Mater. Res. Express., 2019; 6(10): 104003. https://doi.org/10.1088/2053-1591/ab3624
33. Harisha G, Rangaswamy DR, Thejas R, et al. Synthesis and characterization of PANI-CZF nanocomposites for enhanced electromagnetic interference shielding. J. Mater. Sci. Mater. Electron., 2024; 35: 391. https://doi.org/10.1007/s10854-024-12086-6

